PHOTONICS

Organic printed photonics: From microring lasers to integrated circuits

10.1126/sciadv.1500257

Chuang Zhang,[1]* Chang-Ling Zou,[2]* Yan Zhao,[1] Chun-Hua Dong,[2] Cong Wei,[1] Hanlin Wang,[1] Yunqi Liu,[1] Guang-Can Guo,[2] Jiannian Yao,[1†] Yong Sheng Zhao[1†]

A photonic integrated circuit (PIC) is the optical analogy of an electronic loop in which photons are signal carriers with high transport speed and parallel processing capability. Besides the most frequently demonstrated silicon-based circuits, PICs require a variety of materials for light generation, processing, modulation, and detection. With their diversity and flexibility, organic molecular materials provide an alternative platform for photonics; however, the versatile fabrication of organic integrated circuits with the desired photonic performance remains a big challenge. The rapid development of flexible electronics has shown that a solution printing technique has considerable potential for the large-scale fabrication and integration of microsized/nanosized devices. We propose the idea of soft photonics and demonstrate the function-directed fabrication of high-quality organic photonic devices and circuits. We prepared size-tunable and reproducible polymer microring resonators on a wafer-scale transparent and flexible chip using a solution printing technique. The printed optical resonator showed a quality (*Q*) factor higher than 4×10^5, which is comparable to that of silicon-based resonators. The high material compatibility of this printed photonic chip enabled us to realize low-threshold microlasers by doping organic functional molecules into a typical photonic device. On an identical chip, this construction strategy allowed us to design a complex assembly of one-dimensional waveguide and resonator components for light signal filtering and optical storage toward the large-scale on-chip integration of microscopic photonic units. Thus, we have developed a scheme for soft photonic integration that may motivate further studies on organic photonic materials and devices.

INTRODUCTION

Manipulation of photons at the microscale/nanoscale is essential for classical and quantum communicating and computing (*1*–*4*). A variety of materials have been applied to enrich optical functionalities in a broad frequency range (*5*–*7*). Organic conjugated molecules show abundant optical transitions, providing a promising way to achieve active and nonlinear optical properties in photonic circuits. Organic materials take advantage of the outstanding flexibility and compatibility compared to traditional semiconductors, making them an ideal candidate for multifunctional "soft photonics" (*8*, *9*). However, there is an urgent demand for a universal fabrication technique (*10*, *11*) to obtain reproducible organic photofunctional device geometries (*12*, *13*), as photolithography is to silicon-based photonics. Low-dimensional organic structures have been successfully applied in nanolasers, optical waveguides, and logical units for photonic integration (*14*–*17*). Assembling all of these units into a practical photonic circuit (*18*, *19*) requires the fabrication of highly ordered organic microstructures on a universal photonic chip (*20*, *21*). Jet printing has been used to realize large-scale integration in organic flexible electronics and has emerged as a promising method for organic printed photonic integration (*22*).

We report a solution-processed fabrication technique for soft photonic circuits that are integrated from printed optical waveguide and microring resonator structures. One-dimensional (1D) waveguides can transport photons with low optical loss (down to 0.2 dB/mm) as interconnections; microring resonators (with *Q* factors higher than 4×10^5) can effectively confine interior photons to enhance light-matter interaction in circuits. We demonstrated low-threshold microring lasers that can act as an on-chip coherent light source. Light signals can be further manipulated using programmable printed photonic circuits to realize desired functionalities such as light filtering and optical storage. These printable chips are compatible with various dopants and thus can be used in active, nonlinear, electro-optical, and magneto-optical devices (*23*, *24*), which also benefit from the high flexibility, chemical versatility, and widely tunable properties of organic photonic materials.

RESULTS

Organic microstructure patterns were obtained by printing solvent droplets on a polymer thin film (see Materials and Methods and fig. S1) (*11*). The coffee-ring effect (*25*) enabled jetted droplets to partially dissolve the polymer film, resulting in higher ring-shaped structures at the boundary of droplets on the substrate (Fig. 1A). The process included the local dissolution of the micrometer-sized film and the sequential rebuilding of the microstructure, and can be applied to most of the soluble polymers on various substrates (fig. S2). Microrings had a typical radius of ~50 μm, a width of ~5 μm, and a height of about 500 nm. In addition to the microrings, straight microwires for optical waveguiding were also printed (fig. S3). Therefore, this strategy can be used to program arrays of photonic structures on a wafer. Figure 1B shows that the films can be peeled off as free-standing flexible photonic chips for 3D integration and hybridization with other systems. The microscopic structures therein can be patterned over several centimeters (Fig. 1, C and D). The atomic force microscopy (AFM) image in Fig. 1E (see also fig. S4) shows that the surface roughness of these highly uniform microstructures is <1 nm, which benefits from the self-assembly of polymer chains under the surface tension of solvent droplets.

[1]Beijing National Laboratory for Molecular Sciences, Institute of Chemistry, Chinese Academy of Sciences, Beijing 100190, China. [2]Key Laboratory of Quantum Information, University of Science and Technology of China, Hefei 230026, Anhui, China.
*These authors contributed equally to this work.
†Corresponding author. E-mail: yszhao@iccas.ac.cn (Y.S.Z.); jnyao@iccas.ac.cn (J.Y.)

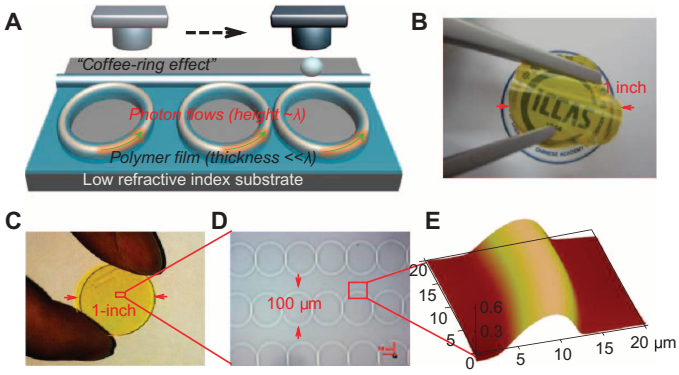

Fig. 1. Design and fabrication of a wafer-scale organic printed photonic chip. (**A**) Schematic of the fabrication of a photonic circuit by confining photon flows in printed structures. A thin film was spin-coated from a polymer solution and locally dissolved by printing solvent droplets, resulting in various microscale structures for light transport. (**B**) Image of a free-standing photonic chip peeled off from the substrate, indicating the flexibility and transparency of the printed photonic chip. A yellow-dye compound was doped into the chip film. (**C**) Image of large-scale ordered optical structures on a 1-inch wafer. (**D**) Microscope image showing printed microring chains of uniform size and well-defined pattern. (**E**) AFM image of a typical self-assembled polymer structure after printing showing the smoothness and height of the structure over the surrounding film.

The highly smooth surface allows for efficient light confinement in as-prepared polymer structures. Thus, the spatial resolution of the printing technique is crucial for guiding internal light transport and other related photonic performances (see Size control of printed structures in the Supplementary Materials). We found that the size (radius, width, and height) of the microrings can be readily controlled by printing on films of different thicknesses (fig. S5) and/or by changing the volume of jetted solvent droplets (fig. S6). All of these microrings are highly reproducible (with a uniform size on the same chip) and show a naturally formed quasi-parabolic shape on the cross section despite the size variation (fig. S7). With a 50-μm-diameter nozzle in our experiments, the radius of the rings can be tuned in the range of ~35 to 82 μm, and their width and height can also be modulated accordingly (table S1).

These size-tunable printed structures were highly transparent, uniform, and smooth, minimizing undesirable scattering and resulting in an ultralow optical loss. The intrinsic loss coefficient was estimated to be ~0.2 to 0.3 dB/mm (fig. S8), which was sufficiently low for light transport in high-performance photonic elements at the microscale (*26*). The refractive index of the polymer film (n_{pf} = 1.58) was obviously higher than that of the substrate (n_{sub} = 1.39), thereby enabling efficient light transport in the polymer layer as long as the height of printed structures $h > \lambda/2(n_{pf}^2 - n_{sub}^2)^{1/2} = 0.66\lambda$ for a given wavelength λ. Therefore, visible light (400 to 700 nm) was well confined in the printed structures (with a height higher than ~400 nm), as indicated by the numerical simulation results for optical waveguiding transverse electric (TE) and transverse magnetic (TM) modes (fig. S9). The fundamental modes dominated other high-order modes, and TE modes were better confined in the waveguide. TM modes (vertically polarized) showed stronger light coupling to the substrate n_{sub} (=1.39)>n_{air} (=1), which brought additional energy dissipation during light propagation (fig. S9).

The efficient optical waveguiding in printed polymer structures enabled the fabricated microrings to further confine the guided light as optical resonators. The *Q* factor of the microring cavity was higher than 10^4, making determination of the intrinsic properties of the cavity by free-space characterization difficult. Therefore, we measured near-field passive-mode transmission by applying a fiber taper coupler (Fig. 2A). The incident light from one end of the fiber was coupled to the attached microring, and we found that the entire ring was efficiently illuminated when optical resonance occurred at the incident wavelength. Moreover, in the pair of conjugated microrings that served as coupled resonators (Fig. 2B), the on-resonance/off-resonance states of each ring were controlled individually based on their distinct resonance modes. The resonance modes confined in the microrings produced transmission dips that were measured from the other end of the fiber (Fig. 2C), and the *Q* factor was obtained from the width of these dips. The highest *Q* factor of TE modes was experimentally obtained as 4.33×10^5 (and even rivaled those of silicon-based cavities), which was calculated by dividing the light frequency by the narrow linewidth of the Lorentzian-shaped dip. A series of periodical sharp dips was observed in the transmission spectrum (Fig. 2D), which was attributed to TE resonance modes from the ring resonator. The transmission at resonance wavelength was as low as 0.03, which shows a near-critical coupling between the fiber and the ring. The free-space range of TE modes was ~0.697 nm, and the corresponding group index was 1.414. In comparison, the *Q* factor of TM modes ($Q = 5.4 \times 10^4$) was nearly one order of magnitude lower than that of TE modes because of the light coupling of TM modes to the substrate (fig. S10). Numerical simulation predicted an increased *Q* factor in a larger microring; however, we experimentally observed a maximum of ~4×10^5 in ~100-μm microrings (fig. S11). The *Q* factor in larger rings might be limited by imperfect shape and increased scattering loss. In principle, the *Q* factor could increase up to 10^7 by further optimizing the materials and the fabrication process.

These high-*Q* printed microcavities can significantly enhance light-matter interactions (*27*) and can be used as active photonic components that can generate or modulate light signals for light information processing. Moreover, the high material compatibility of these polymer films enriches their functionalities by doping with various luminescent dyes (*28*) to produce printed light-emitting microrings for use as microlaser components (Fig. 3A). Figure 3B shows that a highly polarized light emission in the radial direction was observed from the dye-doped microring because of the high *Q* factor of TE modes, which was quite different from the unpolarized light fluorescence from the excitation position. Gradually increasing the energy of the pulsed laser produced a series of narrow peaks in the emission spectra from the dye-doped ring (Fig. 3C). Selective amplification of TE modes (with higher *Q* factors compared with TM modes) indicated the occurrence of lasing action at a pump energy of 50 nJ/pulse.

Figure 3D shows that light output from the resonator produced a clear spectral narrowing compared with fluorescence emission at the excitation position, which was attributed to light amplification from the stimulated emission of dye molecules. Lasing-mode space was inversely proportional to ring size owing to the increase in light path in a larger ring. The height and width of the microrings also affected resonance modes, including the linewidth of laser peaks, as well as the emergence of mode splitting and/or high-order modes (fig. S12). The dependence of light output on power (Fig. 3E) reflected the occurrence of radiation processes in the dye-doped resonator. The slope suddenly changed at a threshold of ~40 nJ/pulse because of the stimulated emission. The peak intensity gradually reached saturation even at higher pump

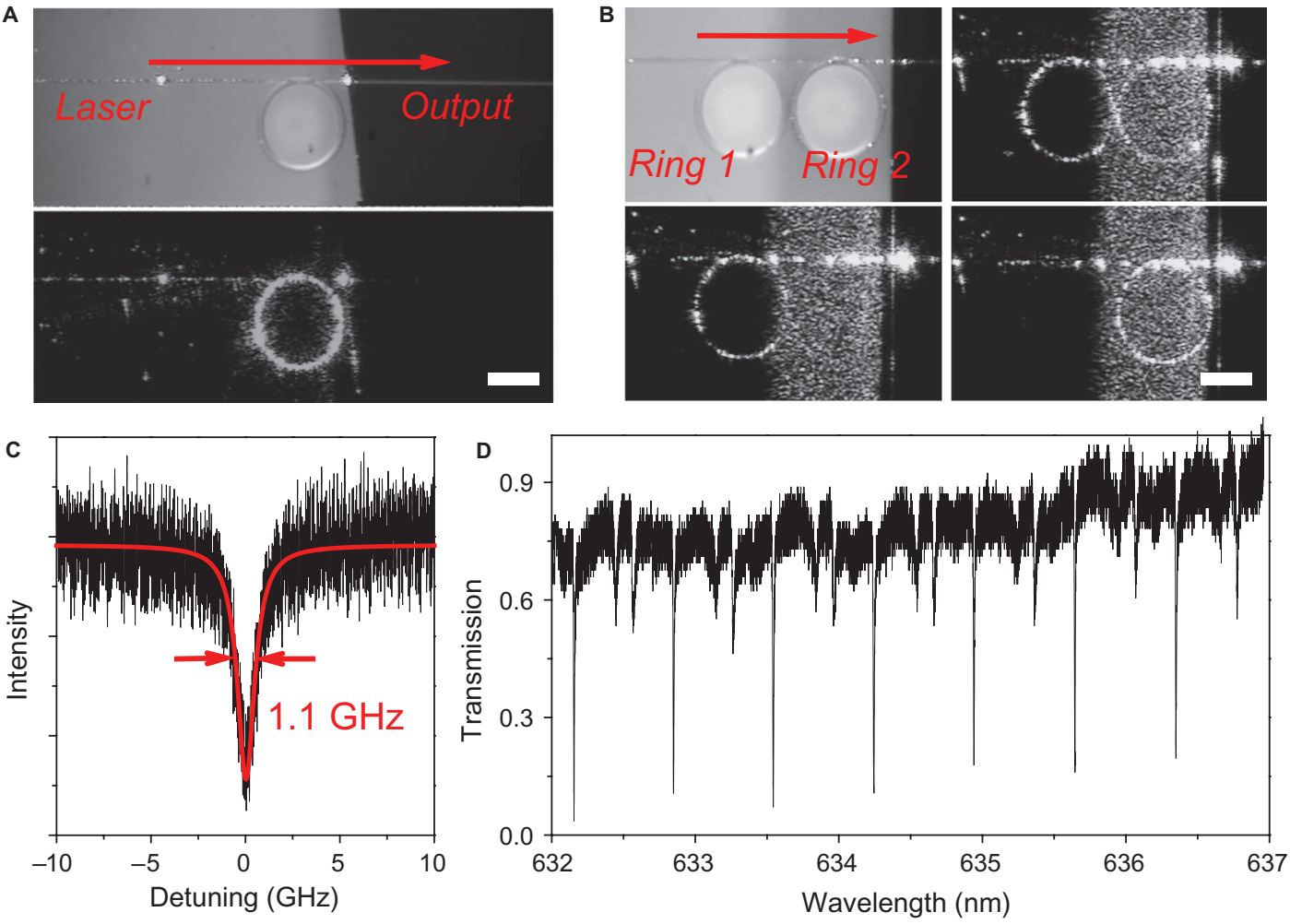

Fig. 2. Characterization of printed microrings as high-*Q* resonators. (**A**) Microscopy image of the structure built for optical measurement. (Top) The optical fiber taper was coupled with a microring at the edge of the film, which was connected to a wavelength-tunable laser at one end and to a photodetector at the other end. (Bottom) The microring was uniformly illuminated when the input wavelength was found at any of its resonance modes. Scale bar, 50 μm. (**B**) Microscopy image of two conjugated microrings coupled with the fiber taper (top left). The incident laser was tuned to the wavelength of the resonance mode of ring 1 and/or ring 2 to illuminate the rings simultaneously (top right) or separately (bottom). Scale bar, 50 μm. (**C**) Frequency detuning profile of the 632.15-nm (~4.75 × 10^5 GHz) resonance mode from the microring resonator with a TE polarized laser. The corresponding *Q* factor is 4.33 × 10^5, as calculated from the frequency of incident light divided by the linewidth of the Lorentz fit (red). (**D**) Broad-range transmission spectrum from the microring, where periodic sharp dips indicate an average *Q* factor higher than 10^5.

powers because the excited states were almost fully occupied under intense excitation. The subsequent variation in energy levels led to a shift in the lasing spectral range, which provides a feasible strategy to actively control coherent light signals by changing excitation power (fig. S13) (*23*). In addition, the reactivity and compatibility of printed organic photonic structures may also provide a means of modulating lasing behavior. For example, we realized a reversible broad-range lasing wavelength shift, together with modulation of laser modes, by exposing the microring laser to the external stimuli of an organic vapor atmosphere (fig. S14). This demonstrated a proof of concept to extend the application areas of printed soft photonic chips, such as photonic sensing with highly sensitive responses to chemical stimuli, which are difficult to do with traditional silicon-based materials. The sensitive nature of soft photonic materials enables us to remotely control the optical performance of fabricated soft photonic devices. Moreover, the lasing spectrum and the stimuli responsiveness might be further broadened by using various gain materials in highly compatible printed microring arrays (fig. S15).

As the microring laser produced initial signals for next-level devices, we explored light signal processing among ring resonators and microwire waveguides (*29*) on the basis of the scalability of printed photonic circuits (see Materials and Methods). Figure 4A shows that ring resonator modes are efficiently coupled into a tangentially connected microwire waveguide, which serves as an on-chip input/output port. The efficient coupling between them results in a highly directional collection of microring resonance modes (Fig. 4B) and thus allows for on-chip modulation of optical resonance in input/output light. The incident light can be selectively confined and can illuminate the microring when its wavelength is found at the resonance of the optical mode (Fig. 2), resulting in the control of output light signals passing through the entire circuit. Therefore, by further designing the arrangement of microrings

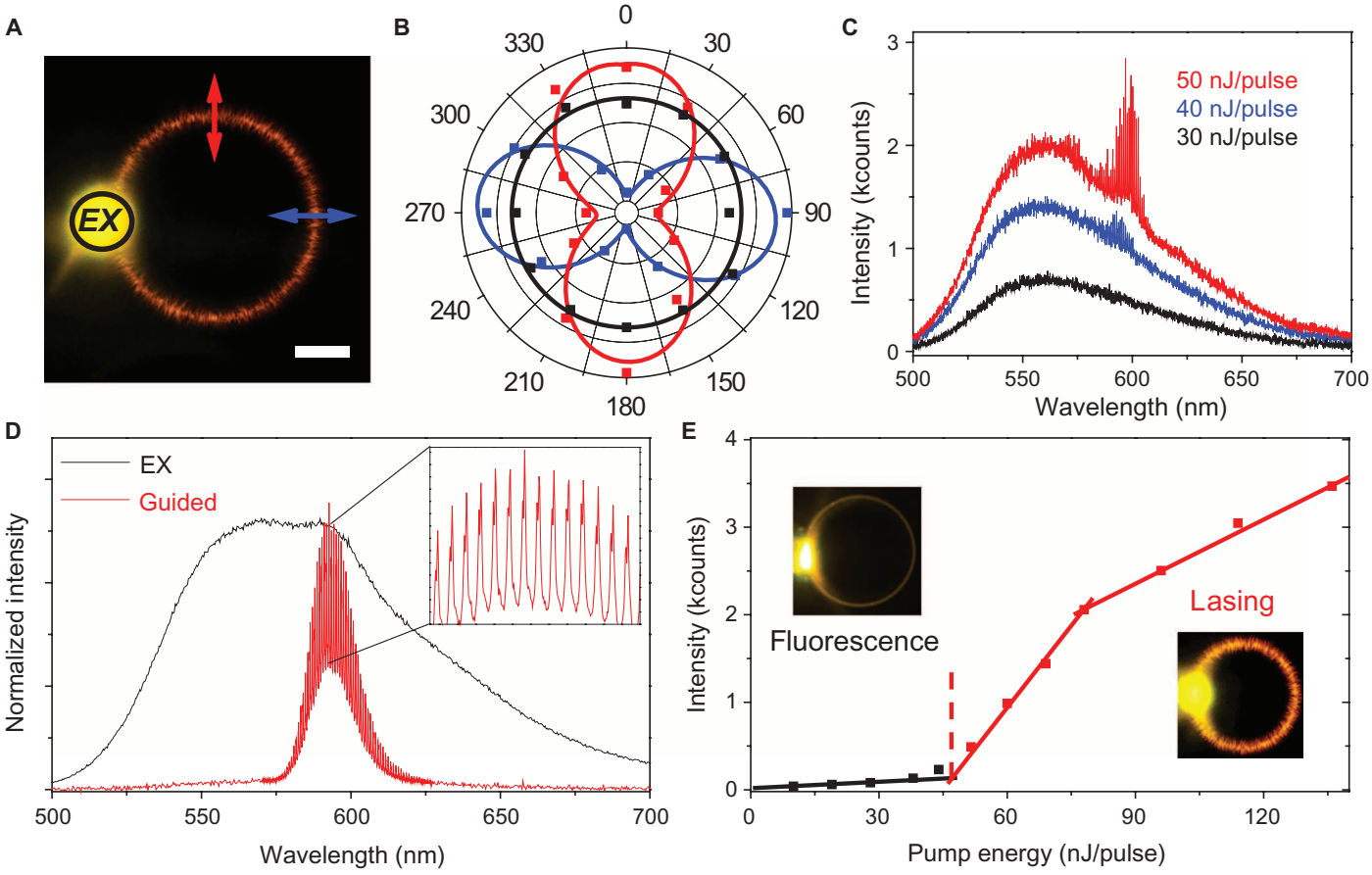

Fig. 3. Low-threshold lasing from dye-doped printed microrings. (**A**) Photoluminescence (PL) microscopy image of a dye-doped microring that was locally excited by a focused 400-nm pulsed laser (~200 fs, 1 kHz). EX, excitation position. Scale bar, 20 μm. (**B**) Spatial polarization profile of light emission from the ring resonator. Collected areas are marked with colored arrows in (A). Polarized PL spectra (red and blue) were ascribed to the outcoupling of TE modes from the ring resonator, whereas the PL spectrum at the EX was unpolarized (black) because of the uncoupled scattering background. (**C**) Output spectra from the entire ring with excitation powers of 30 to 50 nJ/pulse showing the emergence of lasing modes from stimulated emission. (**D**) Spatial spectra of fluorescence scattering at the EX (black) and lasing guided away from the EX (red) showing amplified light emission from resonance modes in the microring. (**E**) Plots of PL peak intensity versus excitation showing the lasing threshold at ~40 nJ/pulse and the nonlinear energy shift at ~80 nJ/pulse. (Insets) Microscopy images of a light-emitting microring below and above the threshold.

and microwires, we can realize the optical processing of different resonance modes on this type of printed chip. Accordingly, we designed and fabricated a light add-drop filter (*30*) composed of three input/output printed 1D waveguide ports and two microring processing modules (Fig. 4C), which can be applied as a multiplexer for the processing of complex light signals (fig. S16). In fact, the compact and scalable add-drop filters fabricated with the printing technique would support running large-scale photonic circuits that can separate light signals at picometer-level spectral resolution (*31*).

The coupling between neighboring printed microrings would enable us to memorize light signals by encoding and selecting the resonance modes (*32*). As shown in Fig. 4D, we studied the light coupling characteristic of two conjugated ring resonators, which, in principle, is a photonic molecule system that is comparable to electron interactions between two atoms. Several resonance modes were enhanced to form newly generated eigenmodes (similar to bonding and antibonding orbitals), and optical modulation was even stronger than that of a single resonator (Fig. 4E); this is known as the Vernier effect (*33*, *34*), which reflects a direct interaction between the optical modes of two nearby resonators. Patterning of more rings into a programmable array would lead to several sharp lines (energy levels) or even continuous band structures around the original mode, with forbidden bandgaps between them over the frequency range. In this context, we fabricated coupled resonator optical waveguides (CROWs) (*35*) on the printed chip, as shown in Fig. 4F. The 2D scalability of a resonator array brings designable collective eigenmodes from the coupling between ring chains in CROWs, providing several distinct energy states (similar to those in an atom cluster) for storing photons (fig. S17). Moreover, dispersion is tailored in CROWs and, thus, group velocity is reduced in light propagation, which is referred to as optical delay or slow light effect. As a result, the light signal could be temporarily memorized in CROWs, which is one of the most important fundamental functionalities in photonic computing.

DISCUSSION

These printed circuits exhibit a considerable potential for applications in integrated optical information processing (*36*). For example, efficient

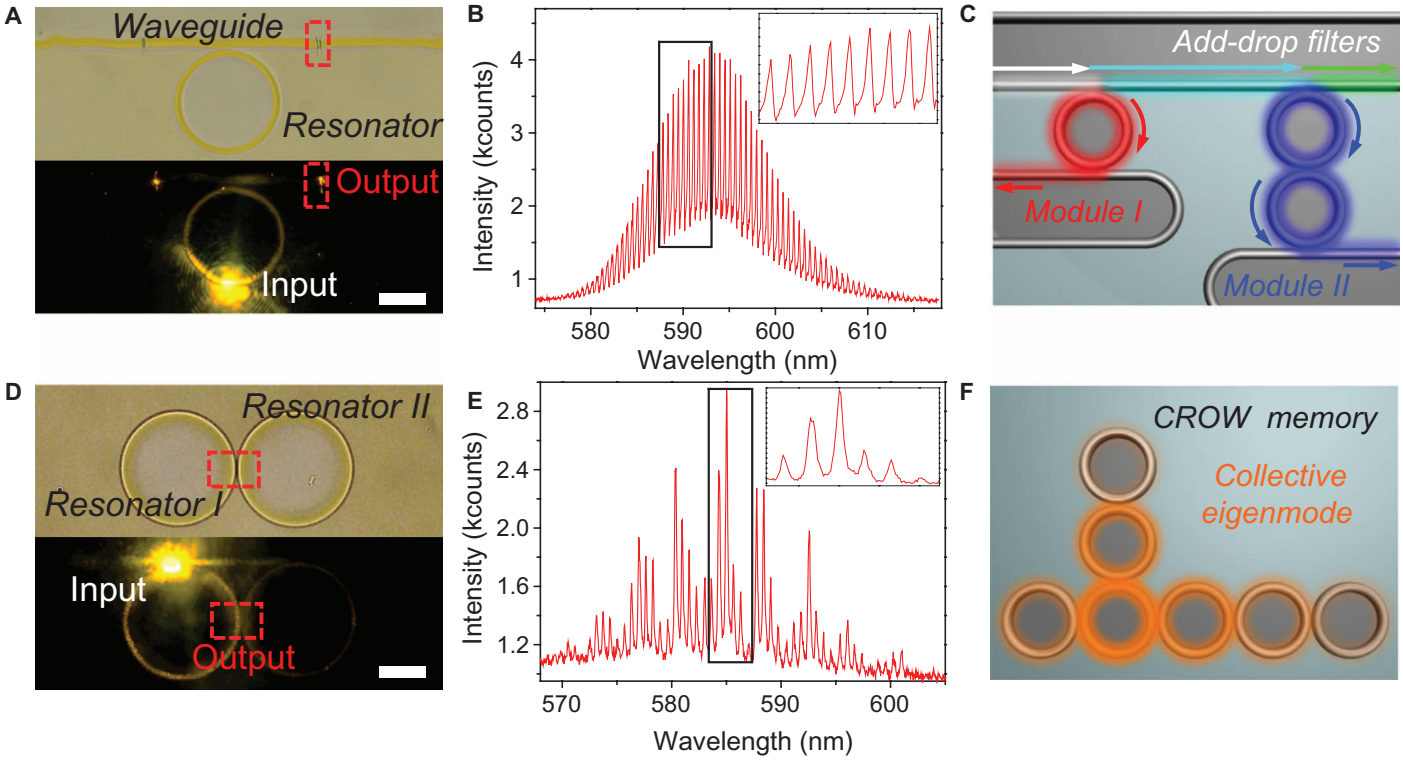

Fig. 4. Organic PICs based on printed microstructures. (**A**) Microscopy image of a printed microring resonator coupled with a tangentially connected 1D waveguide (top) with two laser-burned termini (marked with red rectangles) for light outcoupling. (Bottom) The resonance modes generated by exciting the microring were collected by the waveguide and guided to the termini. (**B**) Corresponding spectrum from the laser-burned slot showing the guided ring resonance modes from the directional output in the coupled optical waveguide. (**C**) Schematic of an as-printed add-drop filter based on the coupling between 1D waveguides and microring resonators. When mixed light signals (white arrow) are inputted from the upper waveguide, the wavelength at resonance (red arrows) is guided into module I, whereas another wavelength goes into module II (blue arrows) on its distinct resonance modes. The signals can thus be distributed into designated ports, and the residual light would pass through the top bus (green arrow). See fig. S12 for details. (**D**) Microscopy image of coupled resonators obtained by printing two conjugated microrings at a distance of ~500 nm (top). (Bottom) The left ring was partially excited, and the right ring was illuminated through resonator coupling. The output spectrum was collected from the point of joining, indicated with a red square. (**E**) Corresponding spectrum shows enhancement of modulated resonance modes from the Vernier effect in coupled cavities. (**F**) Schematic of printed CROWs for optical memory based on programmable printed microring chains. The CROW structure produces a newly generated optical eigenmode (yellow) that can confine photons inside by coupling the resonance modes in each ring. This eigenmode brings isolated states to memorize light signals, similar to energy levels in atom clusters. More eigenmodes at different wavelengths can be obtained from the coupling between vertical ring chains and horizontal ring chains, which are shown in detail in fig. S13.

input/output integration with commercial optical fibers would be realized by matching the refractive indices between organic dielectrics and silica. Printed photonic integrated circuits (PICs) can be fabricated using the same method as for flexible electronics and can thus be combined with optoelectronic components on a single chip. The performance of the proof-of-concept printed PICs presented here might be further improved by optimizing the preparation conditions and device geometries. The multinozzle technique can be further developed, similarly to the color printer, to control the shape and functionality of microstructures. Organic PICs have been realized even on a free-standing flexible soft membrane, which can be layered to form ultrahigh-density 3D photonic circuits. These capabilities would provide further opportunities to observe fascinating optical phenomena and to realize large-scale multifunctional photonic chips (*37*–*39*).

In conclusion, we developed a solution printing technique to fabricate organic photonic structures and devices, thereby paving the way for the realization of flexible high-performance PICs. Printed 1D optical waveguides and microcavities showed low optical losses for light transmission and high *Q* factors in light confinement. The high material compatibility of the printed chip enabled us to realize polarized tunable lasing in microring structures. Light filtering and storage units were integrated on a single chip, indicating the capability of organic printed photonics for light signal processing. The functionality of this type of printed PICs could be increased by simultaneously printing more complex integrations with various doping materials. The strategy demonstrated here could be used to produce numerous organic microphotonic systems, and the results of this study might provide an avenue for high-performance PICs with distinct functionalities.

MATERIALS AND METHODS

Sample preparation

Photonic structures were fabricated on a magnesium fluoride substrate of low refractive index by printing an organic solvent on a polystyrene

film using jet printing (fig. S1). A layer of polystyrene (80, 110, or 200 nm thick) was spin-coated at 3000 rpm from a solution of polystyrene in toluene (10, 30, or 60 mg/ml). *N*,*N*′-Dimethylformamide (DMF) droplets (one droplet is ~65 pl) were jetted using a 50-μm nozzle to etch a ring-shaped structure on the film at 80°C. Straight waveguide structures were prepared by printing solvent droplets continuously in one direction. Morphological parameters were largely tunable by controlling the thickness of the film, the volume of solvent droplets, and other preparation conditions (see also Size control of printed structures in the Supplementary Materials). To fabricate active microring resonators, we added 1,4-bis(*a*-cyano-4-diphenylaminostyryl)-2,5-diphenylbenzene to the polystyrene solution or to the DMF solvent (10 mg/ml) to produce light-emitting doped microrings. The coupled microrings were prepared by precisely moving the nozzle with a step motor (step size ~100 nm), where the second ring was printed ~500 nm from the first ring.

Simulation and characterization

The numerical study of light confinement in the cross section of ring walls was performed by solving Maxwell's equations using the refractive index of the materials. The passive transmission of each microring resonator sample was measured using a coupling fiber taper that was connected to a tunable laser and a detector. The microrings were printed near the edge of the film to facilitate coupling with the fiber. A 400-nm pulsed laser (~200 fs) was focused using a 50× microscope objective to excite the dye-doped ring locally. Spatial photoluminescence was collected and detected by a monochromator that was coupled with a charge-coupled device. A polarizer was used to examine the polarization of light emission from the ring resonator.

SUPPLEMENTARY MATERIALS

Supplementary material for this article is available at http://advances.sciencemag.org/cgi/content/full/1/8/e1500257/DC1

Preparation and characterization of printed optical structures

Fig. S1. Schematic of the fabrication of photonic microring patterns by jet printing.

Fig. S2. Optical microscopy images of microring patterns prepared using various polymers on different substrates.

Fig. S3. Microscopy images of microwires printed by continuous solvent jetting.

Fig. S4. AFM image and roughness profile of the surface of printed microring structures.

Size control of printed structures

Fig. S5. Optical microscopy images of microring structures printed on polymer films of different thicknesses.

Fig. S6. Optical microscopy images of microring structures printed by jetting different volumes of DMF solvent.

Fig. S7. AFM images of printed microrings.

Table S1. Structural parameters of microrings prepared under different conditions.

Performance evaluations of printed optical waveguides and microrings

Fig. S8. Characterization of low optical loss in printed optical waveguides.

Fig. S9. Numerical simulation of the optical waveguiding of TE and TM modes in printed structures.

Fig. S10. Light confinement of TM modes in a microring resonator.

Fig. S11. Theoretical and experimental *Q* factor versus ring radius in microring resonators.

Lasing behavior of dye-doped microring resonators

Fig. S12. Lasing spectra of microring resonators of different sizes.

Fig. S13. Power-dependent modulation of a lasing spectral shift in dye-doped ring resonators.

Fig. S14. Modulation of a microring laser with the external stimuli of acetone vapor.

Fig. S15. Fabrication of microring laser arrays with a broad spectral range by doping different gain media in jetting solutions.

Light signal processing and optical memory in the printed photonic structures

Fig. S16. Light add-drop filter assembled from designed waveguides and microring structures on a printed photonic chip.

Fig. S17. Printed CROWs with two coupled microring chains for eigenmode optical memory.

References (*40*–*50*)

REFERENCES AND NOTES

1. S. D. Smith, Lasers, nonlinear optics and optical computers. *Nature* **316**, 319–324 (1985).
2. J. L. O'Brien, A. Furusawa, J. Vučković, Photonic quantum technologies. *Nat. Photon.* **3**, 687–695 (2009).
3. R. Yan, P. Pausauskie, J. Huang, P. Yang, Direct photonic–plasmonic coupling and routing in single nanowires. *Proc. Natl. Acad. Sci. U.S.A.* **106**, 21045–21050 (2009).
4. M. Law, D. J. Sirbuly, J. C. Johnson, J. Goldberger, R. J. Saykally, P. Yang, Nanoribbon waveguides for subwavelength photonics integration. *Science* **305**, 1269–1273 (2004).
5. C. J. Barrelet, A. B. Greytak, C. M. Lieber, Nanowire photonic circuit elements. *Nano Lett.* **4**, 1981–1985 (2004).
6. W. L. Barnes, A. Dereux, T. W. Ebbesen, Surface plasmon subwavelength optics. *Nature* **424**, 824–830 (2003).
7. D. J. Sirbuly, M. Law, P. Pauzauskie, H. Yan, A. V. Maslov, K. Knutsen, C. Z. Ning, R. J. Saykally, P. Yang, Optical routing and sensing with nanowire assemblies. *Proc. Natl. Acad. Sci. U.S.A.* **102**, 7800–7805 (2005).
8. J. Clark, G. Lanzani, Organic photonics for communications. *Nat. Photon.* **4**, 438–446 (2010).
9. C. Koos, P. Vorreau, T. Vallaitis, P. Dumon, W. Bogaerts, R. Baets, B. Esembeson, I. Biaggio, T. Michinobu, F. Diederich, W. Freude, J. Leuthold, All-optical high-speed signal processing with silicon–organic hybrid slot waveguides. *Nat. Photon.* **3**, 216–219 (2009).
10. R. T. Chen, Polymer-based photonic integrated circuits. *Opt. Laser Technol.* **25**, 347–365 (1993).
11. L. Zhang, H. Liu, Y. Zhao, X. Sun, Y. Wen, Y. Guo, X. Gao, C. A. Di, G. Yu, Y. Liu, Inkjet printing high-resolution, large-area graphene patterns by coffee-ring lithography. *Adv. Mater.* **24**, 436–440 (2012).
12. H. Yanagi, T. Morikawa, Self-waveguided blue light emission in *p*-sexiphenyl crystals epitaxially grown by mask-shadowing vapor deposition. *Appl. Phys. Lett.* **75**, 187–189 (1999).
13. K. Takazawa, J. Inoue, K. Mitsuishi, T. Takamasu, Micrometer-scale photonic circuit components based on propagation of exciton polaritons in organic dye nanofibers. *Adv. Mater.* **23**, 3659–3663 (2011).
14. F. Balzer, V. G. Bordo, A. C. Simonsen, H.-G. Rubahn, Optical waveguiding in individual nanometer-scale organic fibers. *Phys. Rev. B* **67**, 115408 (2003).
15. D. O'Carroll, I. Lieberwirth, G. Redmond, Microcavity effects and optically pumped lasing in single conjugated polymer nanowires. *Nat. Nanotechnol.* **2**, 180–184 (2007).
16. Y. Yan, Y. S. Zhao, Organic nanophotonics: From controllable assembly of functional molecules to low-dimensional materials with desired photonic properties. *Chem. Soc. Rev.* **43**, 4325–4340 (2014).
17. C. Zhang, Y. Yan, Y. S. Zhao, J. Yao, From molecular design and materials construction to organic nanophotonic devices. *Acc. Chem. Res.* **47**, 3448–3458 (2014).
18. F. Di Benedetto, A. Camposeo, S. Pagliara, E. Mele, L. Persano, R. Stabile, R. Cingolani, D. Pisignano, Patterning of light-emitting conjugated polymer nanofibres. *Nat. Nanotechnol.* **3**, 614–619 (2008).
19. Y. Yan, C. Zhang, J. Yao, Y. S. Zhao, Recent advances in organic one-dimensional composite materials: Design, construction, and photonic elements for information processing. *Adv. Mater.* **25**, 3627–3638 (2013).
20. G. M. Whitesides, B. Grzybowski, Self-assembly at all scales. *Science* **295**, 2418–2421 (2002).
21. D. Ammermann, C. Rompf, W. Kowalsky, Photonic devices based on crystalline organic semiconductors for optoelectronic integrated circuits. *Jpn. J. Appl. Phys.* **34**, 1293 (1995).
22. H. Sirringhaus, T. Kawase, R. H. Friend, T. Shimoda, M. Inbasekaran, W. Wu, E. P. Woo, High-resolution inkjet printing of all-polymer transistor circuits. *Science* **290**, 2123–2126 (2000).
23. M. D. McGehee, A. J. Heeger, Semiconducting (conjugated) polymers as materials for solid-state lasers. *Adv. Mater.* **12**, 1655–1668 (2000).
24. S. Kéna-Cohen, S. R. Forrest, Room-temperature polariton lasing in an organic single-crystal microcavity. *Nat. Photon.* **4**, 371–375 (2010).
25. R. D. Deegan, O. Bakajin, T. F. Dupont, G. Huber, S. R. Nagel, T. A. Witten, Capillary flow as the cause of ring stains from dried liquid drops. *Nature* **389**, 827–829 (1997).
26. K. J. Vahala, Optical microcavities. *Nature* **424**, 839–846 (2003).
27. S. M. Spillane, T. J. Kippenberg, K. J. Vahala, Ultralow-threshold Raman laser using a spherical dielectric microcavity. *Nature* **415**, 621–623 (2002).
28. X. Li, N. Gao, Y. Xu, F. Li, Y. Ma, Self-cavity laser oscillations with very low threshold from a symmetric organic crystal waveguide. *Appl. Phys. Lett.* **101**, 063301 (2012).
29. F. C. Blom, D. R. van Dijk, H. J. W. M. Hoekstra, A. Driessen, T. J. A. Popma, Experimental study of integrated-optics microcavity resonators: Toward an all-optical switching device. *Appl. Phys. Lett.* **71**, 747–749 (1997).
30. S. T. Chu, B. E. Little, W. Pan, T. Kaneko, S. Sato, Y. Kokubun, An eight-channel add-drop filter using vertically coupled microring resonators over a cross grid. *IEEE Photon. Tech. Lett.* **11**, 691–693 (1999).
31. L. Fan, J. Wang, L. T. Varghese, H. Shen, B. Niu, Y. Xuan, A. M. Weiner, M. Qi, An all-silicon passive optical diode. *Science* **335**, 447–450 (2012).
32. M. Bayer, T. Gutbrod, J. P. Reithmaier, A. Forchel, T. L. Reinecke, P. A. Knipp, A. A. Dremin, V. D. Kulakovskii, Optical modes in photonic molecules. *Phys. Rev. Lett.* **81**, 2582 (1998).
33. L. Shang, L. Liu, L. Xu, Single-frequency coupled asymmetric microcavity laser. *Opt. Lett.* **33**, 1150–1152 (2008).

34. H. Gao, A. Fu, S. C. Andrews, P. Yang, Cleaved-coupled nanowire lasers. *Proc. Natl. Acad. Sci. U.S.A.* **110**, 865–869 (2013).
35. T. J. Kippenberg, R. Holzwarth, S. A. Diddams, Microresonator-based optical frequency combs. *Science* **332**, 555–559 (2011).
36. M. Hafezi, S. Mittal, J. Fan, A. Migdall, J. M. Taylor, Imaging topological edge states in silicon photonics. *Nat. Photon.* **7**, 1001–1005 (2013).
37. L. K. van Vugt, B. Piccione, C. H. Cho, P. Nukala, R. Agarwal, One-dimensional polaritons with size-tunable and enhanced coupling strengths in semiconductor nanowires. *Proc. Natl. Acad. Sci. U.S.A.* **108**, 10050–10055 (2011).
38. B. Peng, Ş. K. Özdemir, F. Lei, F. Monifi, M. Gianfreda, G. L. Long, S. Fan, F. Nori, C. M. Bender, L. Yang, Parity–time-symmetric whispering-gallery microcavities. *Nat. Phys.* **10**, 394–398 (2014).
39. L. Chang, X. Jiang, S. Hua, C. Yang, J. Wen, L. Jiang, G. Li, G. Wang, M. Xiao, Parity–time symmetry and variable optical isolation in active–passive-coupled microresonators. *Nat. Photon.* **8**, 524–529 (2014).
40. P. J. Yunker, T. Still, M. A. Lohr, A. G. Yodh, Suppression of the coffee-ring effect by shape-dependent capillary interactions. *Nature* **476**, 308–311 (2011).
41. H. Hu, R. G. Larson, Evaporation of a sessile droplet on a substrate. *J. Phys. Chem. B* **106**, 1334–1344 (2002).
42. V. Percec, C.-H. Ahn, G. Ungar, D. J. P. Yeardley, M. Möller, S. S. Sheiko, Controlling polymer shape through the self-assembly of dendritic side-groups. *Nature* **391**, 161–164 (1998).
43. C.-L. Zou, F.-W. Sun, Y.-F. Xiao, C.-H. Dong, X.-D. Chen, J.-M. Cui, Q. Gong, Z.-F. Han, G.-C. Guo, Plasmon modes of silver nanowire on a silica substrate. *Appl. Phys. Lett.* **97**, 183102 (2010).
44. C.-H. Dong, F.-W. Sun, C.-L. Zou, X.-F. Ren, G.-C. Guo, Z.-F. Han, High-*Q* silica microsphere by poly(methyl methacrylate) coating and modifying. *Appl. Phys. Lett.* **96**, 061106 (2010).
45. R. C. Polson, G. Levina, Z. V. Vardeny, Spectral analysis of polymer microring lasers. *Appl. Phys. Lett.* **76**, 3858–3860 (2000).
46. N. Tessler, G. J. Denton, R. H. Friend, Lasing from conjugated-polymer microcavities. *Nature* **382**, 695–697 (1996).
47. I. D. W. Samuel, G. A. Turnbull, Organic semiconductor lasers. *Chem. Rev.* **107**, 1272–1295 (2007).
48. B. E. Little, S. T. Chu, H. A. Haus, J. Foresi, J.-P. Laine, Microring resonator channel dropping filters. *J. Lightwave Technol.* **15**, 998–1005 (1997).
49. T. Barwicz, M. A. Popovic, P. T. Rakich, M. R. Watts, H. A. Haus, E. P. Ippen, H. I. Smith, Microring-resonator–based add-drop filters in SiN: Fabrication and analysis. *Opt. Express* **12**, 1437–1442 (2004).
50. H. Takesue, N. Matsuda, E. Kuramochi, W. J. Munro, M. Notomi, An on-chip coupled resonator optical waveguide single-photon buffer. *Nat. Commun.* **4**, 2725 (2013).

Acknowledgments: We thank H. Tang (Yale University), L. Jiang (Yale University), and L. Yang (Washington University, St. Louis) for fruitful discussions. **Funding:** This work was supported by the National Natural Science Foundation of China (grants 21125315 and 21221002), the Ministry of Science and Technology of China (grant 2012YQ120060), and the Strategic Priority Research Program of the Chinese Academy of Sciences (grant XDB12020300). **Author contributions:** Y.S.Z. conceived the original concept. C.Z., C.-L.Z., and Y.S.Z. designed the experiments. Y.Z., C.Z., C.W., and H.W. fabricated the printed structures. C.-H.D. measured *Q* factors and the transmission spectra of microring resonators. C.Z. and C.W. measured optical waveguiding and lasing from the printed structures. C.-L.Z. performed simulations of light confinement and *Q* factors. C.Z., C.-L.Z., and Y.S.Z. analyzed the data and wrote the manuscript. All authors discussed the results and contributed to the manuscript. **Competing interests:** The authors declare that they have no competing interests. **Data and materials availability:** Data will be made available upon request by emailing yszhao@iccas.ac.cn.

Submitted 27 February 2015
Accepted 23 June 2015
Published 18 September 2015
10.1126/sciadv.1500257

Citation: C. Zhang, C.-L. Zou, Y. Zhao, C.-H. Dong, C. Wei, H. Wang, Y. Liu, G.-C. Guo, J. Yao, Y. S. Zhao, Organic printed photonics: From microring lasers to integrated circuits. *Sci. Adv.* **1**, e1500257 (2015).